High-pressure phase transitions of forsterite from first-principles

A. Bouibes, Ali Zaoui

High-pressure phase transitions of Forsterite from first-principles

A. Bouibes and A. Zaoui*

LGCgE, Polytech'Lille, Univ. Lille 1 Sciences and Technologies. Cite Scientifique, Avenue Paul Langevin, 59655 Villeneuve d'Ascq, France.

Abstract

From *ab initio* evolutionary algorithm, we predict a new high pressure phase transition of Mg_2SiO_4 (Forsterite) above 30 GPa. At this pressure, Forsterite changes into post-spinel structure with *Pbam* space group. This structure has attracted the interest of many previous works, but which have not been definitively conclusive. Forsterite is stabilized under further phase transition at 64.5 GPa. Above this pressure, the structure with C$mc2_1$ space group becomes the most stable.

Keywords: Forsterite; DFT; High pressure; Structural properties.

*Email address: azaoui@polytech-lille.fr

The modern first-principles calculation technique is a reliable tool for studying the electronic structure of materials under extreme conditions, such as high pressure and temperature. By performing *ab initio* simulations one can go far beyond the pressure and temperature range achieved experimentally. An important area, which can be dealt by using first-principles calculations, is the study of the structural stability and phase transformations at high pressure of Earth's interior constituents [1]. The most important constituents of Earth are silicates which constitute 95 percent of the rocks of the Earth's crust. They are considered as dominant mineral phase of Earth's upper mantle, which occur widely in igneous and metamorphic rocks [2-3]. In addition, these minerals could be found in other planets [4]. The most astrophysically important silicate groups are olivines and pyroxenes [5]. Olivines are characterized to have the $[SiO_4]^{4-}$ tetrahedra linked by Mg^{2+} and Fe^{2+} and the general formula $Mg_{2x}Fe_{(2-2x)}SiO_4$ (x = 0–1), with the two end members named forsterite (Mg_2SiO_4) and fayalite (Fe_2SiO_4) [5]. Whereas, pyroxenes are formed by single chains of $[SiO_4]^{4-}$ intercalated by the divalent cations and have the general formula $Mg_xFe_{(1-x)}SiO_3$ (x = 0–1)[5]. This ferromagnesian pyroxene seems to have implications for enigmatic seismic feature beyond 2000 Km. Indeed, $(Mg,Fe)SiO_3$ is unstable in the temperature and pressure higher than 2200 K and 95 GPa respectively, and forms Fe-free $MgSiO_3$ perovskite phase and a Fe-riche phase with a hexagonal structure [6]. On the other hand, the phase transitions in Mg-rich olivine and its polymorphs are believed to be responsible for the major seismic discontinuities at 410, 520, and 660 km depth [3]. Olivine's creep behavior exerts a major control on mantle rheology and affects the interpretation of seismic anisotropy [7]. While olivine transforms to wadsleyite at a depth near 410 km (~14GPa) at normal mantle temperatures, it may persists metastably in cold subducting lithosphere below 410 km depth and plays a role in deep earthquake generation [8-9]. There has also been interest in the behavior of amorphous and liquid Mg_2SiO_4 over a wide range of pressures as a model system for understanding partial melting of the mantle, production of basalts and komatiites, and the behavior of magma oceans [10-12].

The question of stability of olivine at the Earth's mantles condition arose a great interest to researchers, where a series of experiments as well as theoretical investigations, have been carried out [2-12]. The structure of Olivine has been found experimentally and theoretically at ambient conditions [12-17]. The Olivine structure has P*bnm* space group and Z=4 formula with 28 atom in unit cell. It can be described as an expanded and distorted hexagonally close-packed (hcp) array of oxygen anions stacked along the a direction. Si cations are situated in tetrahedral sites, and Mg is in two distinct octahedral sites; Si-O tetrahedral are isolated and share corners with Mg-O octahedral, while the Mg-O octahedral sharer both corners and

edges. There are three distinct oxygen: O1 and O2 are located on a mirror plane, while O3 is in a general position. Each oxygen anion is bonded to three octahedral cations and one tetrahedral cation [12-13].

Under pressure, several theoretical and experimental studies report that the Olivine becomes metastable above 14GPa and take other forms. Wadsleyite and ringwoodite are reported to be the main forms of Mg_2SiO_4 at high pressure. These polymorphs are denoted as β- and γ-Mg_2SiO_4 phase, respectively. The phase transition, between β-Mg_2SiO_4 and γ-Mg_2SiO_4 phases, occurs around 17 GPa (520 Km depth). The transitions between these olivine phases induced by pressure and also temperature, the reported thermodynamic stable phase of Forsterite are presented in shematic phase pressure–temperature diagram in Fig.1 [14-20]. Recently, Finkelstein *et al.* investigated different phase transitions of Forsterite using single crystal X-ray diffraction and molecular modeling [12]. They revealed that Forsterite knows two phase transitions up to 90 GPa of pressure. The first one at 50 GPa, and the second one at 58 GPa. Before 50 GPa, Forsterite is stable under P*bnm* space group structure, and between 50GPa and 58 GPa Forsterite stabilizes in P1 space group structure. Above 58 GPa, Forsterite is stable into C$mc2_1$ space group structure [12]. We report here the new phase transitions to Forsterite at high pressure. To this end, we have used *ab initio* structures prediction.

In order to find the stable high-pressure structures of Forsterite, an *ab initio* evolutionary algorithm (EA), as implemented in the "Universal Structure Predictor: Evolutionary Xtallography" (USPEX) code, is employed [25-28]. The local optimization of the candidate structures were carried out using density functional theory (DFT) calculations with the generalized gradient approximation (GGA), and the Perdew–Burke–Ernzerhof (PBE) [29] exchange-correlation functional, as implemented in the Vienna *ab-initio* Simulation Package (VASP) code [30-31]. The structure prediction of Mg_2SiO_4 was performed at 1atm, 20GPa, 50 GPa, 55GPa, 70 GPa, 100GPa, 125GPa, 150 GPa all at zero Kelvin. In these variable-cell simulations, we consider the system with 14 and 28 atoms in the unit cell. The population size is fixed at 40 numbers of structures. Forsterite II found by Finkelstein et al. at 1000K and also Wadsleyite structure with 56 atoms in unit cell were added to the resulting structures [12,15].

The structural and mechanical properties of the obtained structures were calculated using PBE-D2 exchange-correlation functional with D2 dispersion correction (PBE-D2)[32], as implemented in VASP code [30-31] . We used the all-electron projector-augmented wave (PAW) [33]. The plane-wave kinetic-energy cutoff is 900 eV, and the k-point mesh resolution in reciprocal space is 2*0.03 A^{-1}. These settings enable excellent convergences of the energy differences, stress tensors, and structural parameters.

In Fig.2, enthalpies of the obtained structures relative to the enthalpy of the forsterite phases versus pressure are shown. One can see immediately from Fig.2.a that the P1 space group structure, reported by Finkelstein *et al* as Forsterite phase II, is metastable at 0K within the whole range of applied pressure, and one may disregard it from further consideration.

The most stable structure of Mg_2SiO_4 at ambient conditions is the P*bnm* space group structure called α-Mg_2SiO_4, which fits perfectly the experiment [12]. The obtained lattice parameters as well as bulk modulus and its derivative are summarized in Table 1.

By comparing the enthalpies of the remaining structures, we estimated pressures at which phase transitions occurs. Fig.2.b. shows the first and second phase transition pressures. The first transition from Forsterite Phase I to Forsterite phase II structure occurs at 12.6 GPa. The second one occurs at 16.3 GPa. The Forsterite phase II and phase III are β-wadsleyite structure, which has Imma space group, and ringwoodite (γ-spinel) structure, with Fd-3m space group, respectively. The obtained lattice parameters as well as bulk modulus and its pressure derivative of the optimized Forsterite phase III, at ambient conditions, are summarized in Table 2. These results fit perfectly previous several theoretical and experimental studies [13-23].

By increasing pressure, Forsterite phase III is stable until 30 GPa where the new third phase transition occurs. Between 30 GPa and 64.5 GPa, the novel most stable structure has a space group *Pbam* including 28 atoms in the primitive cell. The Forsterite phase IV contains octahedral $(SiO_6)^{4-}$ ions in a parallel orientation as we can see in Fig.3.a. In addition, Mg atom are located in octahedral sites. The obtained structural properties as well as bulk modulus and its pressure derivative of the optimized Forsterite phase IV, at ambient conditions, are summarized in Table 3.

Above 64.5 GPa, the structure of $Cmc2_1$ space group becomes more stable as shown in Fig.2.c. Table 4 reported the obtained structural properties of the optimized Forsterite phaseV at ambient conditions as well as the obtained bulk modulus and its pressure derivative from the Birch–Murnaghan equation of state. The Forsterite phase V is presented in Fig.3.b. We can see that Si atom is located in octahedral sites, and Mg1 atoms (yellow color) are located also in octahedral site. However Mg2 atoms (orange color) are located in face –sharing trigonal prism sites. Let us notice that the latter was also found by Finkelstein et al. [12].

In order to confirm our prediction, we studied the dynamical stability of new Forsterite phase IV and V at 50GPa and 70 GPa, respectively. To this end, we applied the Born stability criteria [24]. The Born stability criteria for an orthorhombic system are:

$$B1,ii = Cii > 0 \ (i=1\text{-}6) \qquad (1)$$

$$B2, ij = \begin{vmatrix} Cii & Cij \\ Cji & Cjj \end{vmatrix} > 0 \quad (\text{ij} = \{23\}, \{31\}, \{12\}) \quad (2)$$

$$B3 = \begin{vmatrix} C11 & C12 & C13 \\ C21 & C22 & C23 \\ C31 & C32 & C33 \end{vmatrix} > 0 \quad (3)$$

Table 5 reports the calculated elastic constant of P*bam* structure and $Cmc2_1$ structure at 50 GPa and 70 GPa. The three born criteria are respected. Thus, the predicted structures are dynamically stable.

In conclusion, we have predicted through this study the unknown post-spinel structures above 30 GPa. We have determined the Forsterite phase IV and Forsterite phase V, which are P*bam* space group structure and $Cmc2_1$ space group structure respectively.

References:

[1] Arapan, S., Jailton S., D. A., Rajeev A., Formation of sp^3 Hybridized Bonds and Stability of $CaCO_3$ at Very High Pressure. *Physical review letters* **98**.26: 268501. (2007)

[2] Deer, W. A., Howie, R., A., Zussman J., *Orthosilicates. Longman*. (1982)

[3] Ringwood, A. E. Phase transformations and their bearing on the constitution and dynamics of the mantle. *Geochimica et Cosmochimica Acta* **55**.8: 2083-2110. (1991)

[4] Mustard, J. F. *et al.* Olivine and pyroxene diversity in the crust of Mars". *Science*, **307** (5715), 1594-1597. (2005)

[5] Martínez-González, J., Navarro-Ruiz, J., Rimola, A., Multiscale Computational Simulation of Amorphous Silicates Structural, Dielectric, and Vibrational Spectroscopic Properties. *Minerals* **8**.8: 353. (2018)

[6] Zhang, L., Meng, Y., Yang, W., Wang, L., Mao, W. L., Zeng, Q. S., *et al.*, Disproportionation of $(Mg,Fe)SiO_3$ perovskite in Earth's deep lower mantle. *Science,* 344: 877-882(2014).

[7] Karato, Shun-I., Patrick Wu. Rheology of the upper mantle- A synthesis. *Science* **260**.5109: 771-778. (1993)

[8] Kirby Stephen H, Stein S, Okal E. A, Rubie D.C Metastable mantle phase transformations and deep earthquakes in subducting oceanic lithosphere. *Reviews of Geophysics* **34**: 261-306. (1996)

[9] Kawakatsu, Hitoshi, and Shoichi Yoshioka. Metastable olivine wedge and deep dry cold slab beneath southwest Japan. *Earth and Planetary Science Letters* **303**.1: 1-10. (2011)

[10] de Koker, Nico P., Lars Stixrude, and Bijaya B. Karki. Thermodynamics, structure, dynamics, and freezing of Mg_2SiO_4 liquid at high pressure. *Geochimica et Cosmochimica Acta* **72**.5: 1427-1441. (2008)

[11] Adjaoud, O., G. Steinle-Neumann, Jahn. S., Transport properties of Mg_2SiO_4 liquid at high pressure: Physical state of a magma ocean. *Earth and Planetary Science Letters* **312**.3: 463-470. (2011)

[12] Finkelstein, G. J., Dera, P. K., Jahn, S., Oganov, A. R., Holl, C. M., Meng, Y., Duffy, T. S., Phase transitions and equation of state of forsterite to 90 GPa from single-crystal X-ray diffraction and molecular modeling. *American Mineralogist* **99**(1), 35-43. (2014)

[13] Smyth, Joseph R., Steven D. Jacobsen, and Robert M. Hazen. "Comparative crystal chemistry of orthosilicate minerals. *Reviews in mineralogy and geochemistry* **41**.1: 187-209. (2000)

[14] Guyot, François, and Bruno Reynard. Pressure-induced structural modifications and amorphization in olivine compounds. *Chemical geology* **96**.3: 411-420. (1992)

177 [15] Horiuchi, H., Sawamoto, H., β-Mg_2SiO_4: Single-crystal X-ray diffraction study.
178 *American mineralogist* **66** .: 568-575. (1981)
179 [16] Andrault, D., Bouhifd, M. A., Itie, J. P., Richet, P. Compression and amorphization of
180 $(Mg, Fe)_2SiO_4$ olivines: an X-ray diffraction study up to 70 GPa. *Physics and Chemistry of*
181 *Minerals*, **22**(2), 99-107. (1995)
182 [17] Rouquette, J., Kantor, I., McCammon, C. A., Dmitriev, V., Dubrovinsky, L. S. High-
183 pressure studies of $(Mg_{0.9}Fe_{0.1})_2SiO_4$ olivine using Raman spectroscopy, X-ray diffraction,
184 and Mössbauer spectroscopy. *Inorganic chemistry*, **47**(7), 2668-2673. (2008)
185 [18] Suito, K. Phase transformations of pure Mg_2SiO_4 into a spinel structure under high
186 pressure and temperatures, *Journal of Physics of the Earth* 20, 225-43 (1972).
187 [19] Katsura, T., Ito, E., The system Mg_2SiO_4-Fe_2SiO_4 at high pressures and temperatures:
188 Precise determination of stabilities of olivine, modified spinel, and spinel. *Journal of*
189 *Geophysical Research.* (94) .**B11**, 15663-15670. (1989).
190 [20] Tokar, K., Jochym, P. T., Piekarz, P., Lazewski, J., Sternik, M., Parlinski, K.
191 Thermodynamic properties and phase stability of wadsleyite II. *Physics and Chemistry of*
192 *Minerals*, **40** (3), 251-257. (2013).
193 [21] Inoue, T., Weidner, D. J., Northrup, P. A., Parise, J. B. Elastic properties of hydrous
194 ringwoodite (γ-phase) in Mg_2SiO_4. *Earth and Planetary Science Letters*, **160**, 107-113.
195 (1998).
196 [22] Wentzcovitch, R. M., Yonggang, G. Y., Wu, Z. "Thermodynamic properties and phase
197 relations in mantle minerals investigated by first principles quasiharmonic theory." *Reviews in*
198 *Mineralogy and Geochemistry*, **71**(1), 59-98. (2010).
199 [23] Dziewonski, A. M., Anderson, D. L. "Preliminary reference Earth model." *Physics of the*
200 *earth and planetary interiors*, **25**(4), 297-356. (1981).
201 [24] Born, M., and K. Huang, Dynamical Theory of Crystal Lattices, 432 pp, Oxford
202 University. Press, New York.
203 [25] Oganov, A. R., et al. "Evolutionary crystal structure prediction as a method for the
204 discovery of minerals and materials". *Reviews in Mineralogy and Geochemistry* **71**, 271-298
205 (2010).
206 [26] Oganov, A. R., Glass, C. W. Crystal prediction using *ab initio* evolutionary techniques:
207 Principles and applications. *Journal of Chemical Physics.* **124**, 244704 (2006).
208 [27] Lyakhov, A. O., et al. New developments in evolutionary structure prediction algorithm
209 USPEX. *Computer Physics Communications* **184**, 1172-1182 (2013).
210 [28] Oganov, A. R., et al. How evolutionary crystal structure prediction works – and why.
211 *Accounts of Chemical Research* **44**, 227-237 (2011).

[29] Perdew, J. P. et al. Generalized gradient approximation made simple. *Physical Review letter.* **77**, 3865 (1996).

[30] Kresse, G. and Furthmüller, J. Efficient iterative schemes for *ab initio* total-energy calculations using a plane-wave basis set. *Physical Review B* **54**, 11169 (1996).

[31] Kresse, G. Furthmu¨ller, J. Software VASP, Vienna, *Physical Review B,* **54**, 1996 (1999).

[32] Grimme, S., Semiempirical GGA-type density functional constructed with a long-range dispersion correction. *Journal Computational Chemistry.* **27**: 1787-1799 (2006).

[33] Kresse, G. and Joubert, D. From ultrasoft pseudopotentials to the projector augmented-wave method. *Physical Review B* **59**, 1758 (1999).

[34] Vinet, P., Rose, J. H., Ferrante, J., Smith, J. R., Universal features of the equation of state of solids. *Journal of Physics: Condensed Matter*, **11**, 1941 (1989).

Figure captions

Figure 1: Shematic phase pressure–temperature diagram of Mg_2SiO_4.

Figure2: Enthalpies of the best forsterite structures vs pressure (a), zoom of enthalpies-pressure diagram: from 4 to 22 GPa (b) and from 20 to 80 GPa of pressure (c).

Figure3: Forsterite phase IV (Pbam) at 50 GPa: yellow spheres –Mg atoms, blue spheres-Si atoms, small red spheres – O atoms (a); Forsterite phase V ($Cmc2_1$): : yellow spheres –Mg1 atoms, Orang spheres: Mg2 atoms, blue spheres-Si atoms, small red spheres – O atoms (b).

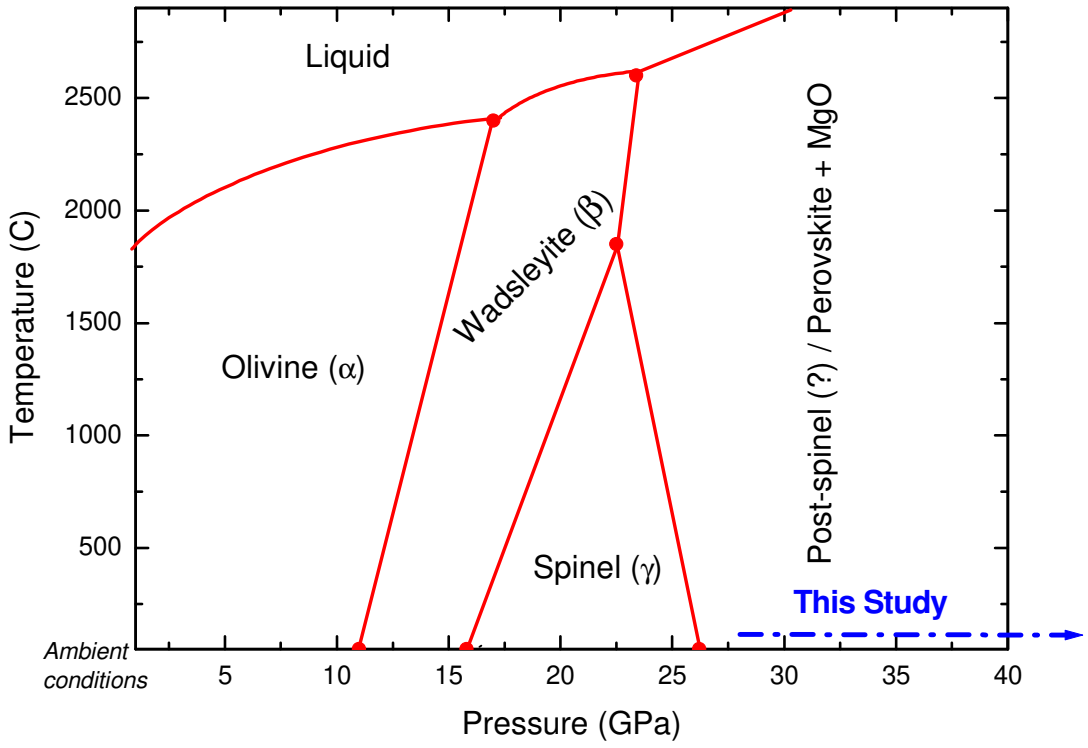
Liquid
Olivine (α)
Wadsleyite (β)
Spinel (γ)
Post-spinel (?) / Perovskite + MgO
This Study
Ambient conditions
Temperature (C)
Pressure (GPa)
2500
2000
1500
1000
500
5
10
15
20
25
30
35
40

Fig.1

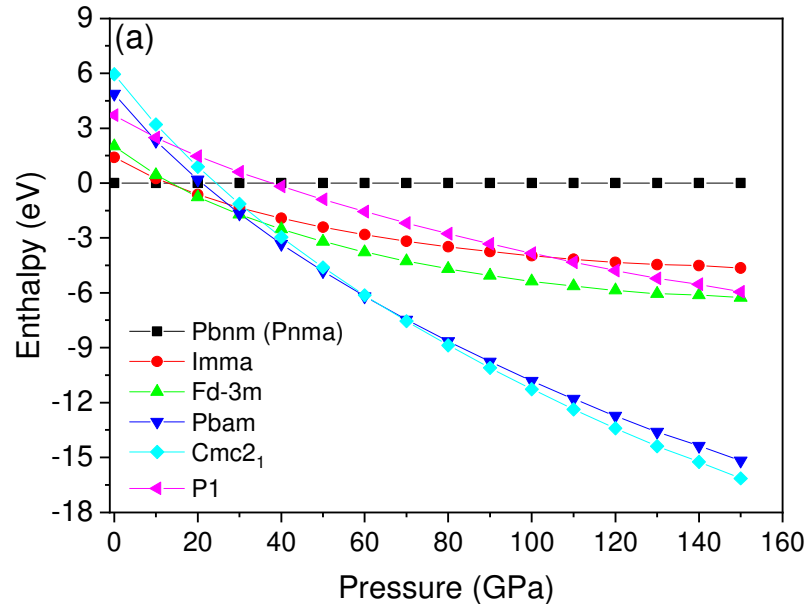
(a)
Enthalpy (eV)
Pressure (GPa)
Pbnm (Pnma)
Imma
Fd-3m
Pbam
Cmc2$_1$
P1

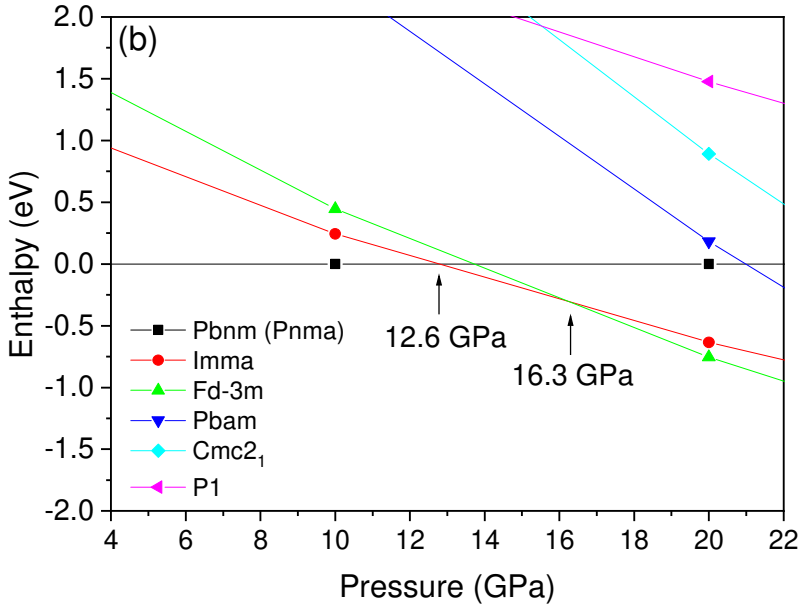
(b)
Enthalpy (eV)
Pressure (GPa)
12.6 GPa
16.3 GPa
Pbnm (Pnma)
Imma
Fd-3m
Pbam
Cmc2$_1$
P1

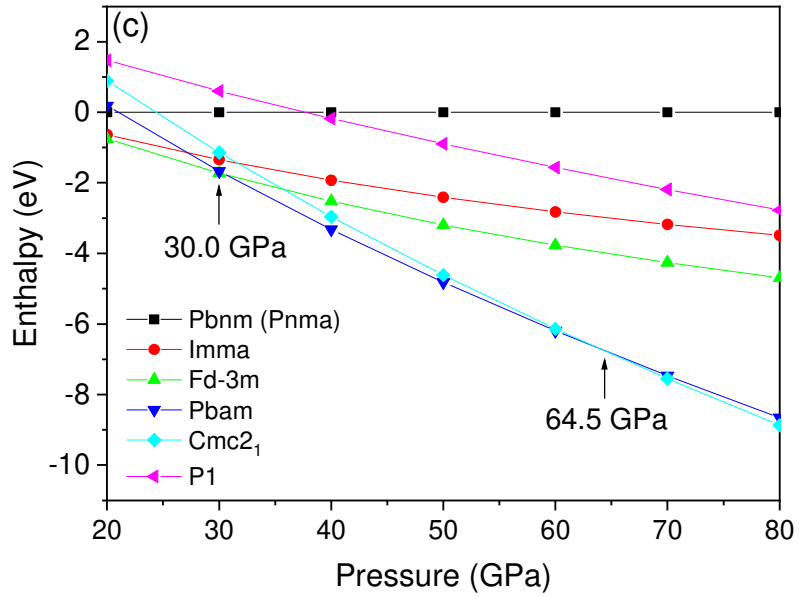
(c)
Enthalpy (eV)
Pressure (GPa)
30.0 GPa
64.5 GPa
Pbnm (Pnma)
Imma
Fd-3m
Pbam
Cmc2$_1$
P1

Fig.2

(a) (b)

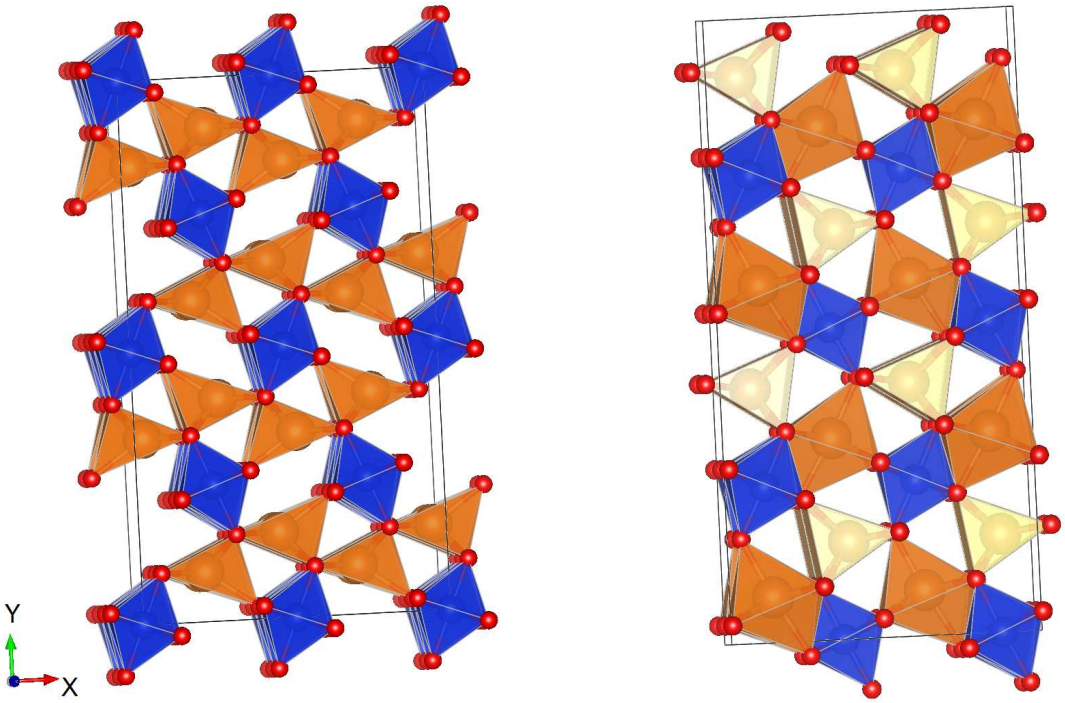

Fig.3

Tables:

Table 1: Obtained forsterite Phase I at ambient conditions.

a (Å)= 10.1750 (10.201)*
b(Å)= 5.9860 (5.9819)*
c(Å)= 4.7910 (4.7543)*
V_0(Å^3)= 291.81 (290.1)*
K_0*(GPa)= 129 GPa (130[a], 128[b], 128.8[c])*
K'$_0$*= 3.8 (4.12[a], 4.0[b], 4.2[c])*
Space group : *Pnma (Pbnm)*

Atoms	**x**	**y**	**z**
Mg1	0.0000	0.0000	0.5000
Mg2	-0.2230	0.2500	-0.0102
Si	-0.4060	0.2500	0.4275
O1	-0.4085	0.2500	-0.2331
O2	-0.0545	0.2500	0.2219
O3	-0.3364	0.0314	0.2769

**Experimental data reference [12]*
[a]Using single-crystal X-ray diffraction
[b]Using polycrystalline X-ray diffraction
[c]Using Brillouin spectroscopy

Table 2: Stable Mg_2SiO_4 structure (Phase III) between 16.3 GPa and 30 GPa, as well as obtained bulk modulus and its derivative according to the Birch–Murnaghan equation of state [34].

a(Å)= 8.0923 (8.129[a], 8.0649±1[b])
V_0(Å^3)= 529.94 (537.16[a], 524.56[b])
K_0 (GPa)= 183.6 GPa (184±2[b])
K'$_0$= 3.8
Space group: *Fd-3m*

Atoms	**x**	**y**	**z**
Mg	0.0000	0.0000	0.0000
Si	0.3750	0.3750	0.3750
O	-0.2556	-0.2556	-0.2556

[a]Experimental data reference [20]
[b]Experimental data reference [21]

Table 3: structural parameters of new stable Mg_2SiO_4 structure (Phase IV) between 30 GPa and 64.5 GPa as well as obtained bulk modulus and its derivative according to the Birch–Murnaghan equation of state [34].

a(Å)=5.0150			
b(Å)=8.8720			
c(Å)=2.8250			
V_0(Å^3)= 125.693			
K_0 (GPa)= 182			
K'$_0$= 3.8			
Space group : *Pbam*			
Atoms	**x**	**y**	**z**
Mg	-0.4379	0.3197	0.0000
Si	0.0000	0.5000	0.5000
O1	-0.2721	0.0470	0.0000
O2	-0.3647	-0.1843	0.5000

Table 4: Stable Mg_2SiO_4 structure (Phase V) above 64.5 GPa.

a(Å)=2.7855			
b(Å)=9.4506			
c(Å)=9.4000			
V_0(Å^3)= 247.4517			
K_0 (GPa)= 197.12			
K'$_0$= 3.4			
Space group : *Cmc2$_1$*			
Atoms	**x**	**y**	**z**
Mg1	0.0000	0.3623	-0.1485
Mg2	0.0000	-0.1084	0.1854
Si	0.0000	-0.3728	-0.0020
O1	0.0000	-0.4555	0.1612
O2	0.0000	-0.2942	-0.1751
O3	0.0000	-0.0058	0.4354
O4	0.0000	-0.2477	-0.4555

336 Table 5: Elastic constants of Forsterite phase IV and V at 50 GPa and 70 GPa respectively.

337

	Pbam	*Cmc2*$_1$
C_{11}	682.24	628.39
C_{22}	467.39	675.34
C_{33}	648.74	769.24
C_{12}	230.47	295.29
C_{13}	121.93	188.17
C_{23}	199.13	189.61

338